Published in final edited form as:
Mater Chem Phys. ; 267: . doi:10.1016/j.matchemphys.2021.124604.

Electrochemical fabrication of TiO_2 micro-flowers for an efficient intracellular delivery using nanosecond light pulse

L. Mohan[#a,b], **Srabani Kar**[#a,c], **Moeto Nagai**[b], **Tuhin Subhra Santra**[a,*]

[a]Department of Engineering Design, Indian Institute of Technology Madras, India

[b]Department of Mechanical Engineering, Toyohashi University of Technology, Japan

[c]Department of Electrical Engineering, University of Cambridge, UK

[#] These authors contributed equally to this work.

Abstract

Introduction of foreign cargo into the targeted living cell with high transfection efficiency and high cell viability is an important mean for many biological and biomedical research purpose. Here, we have demonstrated a newly developed Titanium oxide micro-flower structure (TMS) for intracellular delivery. The TMS were formed on titanium (Ti) substrate using an electrochemical anodization process. The TMS consists of branches of titanium dioxide (TiO_2) nanotubes, which play an important role in efficient cargo delivery. Due to nanosecond pulse laser exposure, Ti substrate heat-up, generating cavitation bubbles. These bubbles can rapidly grow, coalesce, and collapse to induce explosion resulting in very strong fluid flow through the TiO_2 nanotubes and disrupt the cell plasma membrane promoting the delivery of biomolecules into cells. Using this platform, we successfully deliver dyes with 93% efficiency and nearly 98% cell viability into HCT cells, and this technique is potentially applicable for cellular therapy and diagnostics.

Abstract

[*]Corresponding author. tuhin@iitm.ac.in, santra.tuhin@gmail.com (T.S. Santra).

Declaration of competing interest

The authors declare that they have no known competing financial interests or personal relationships that could have appeared to influence the work reported in this paper.

Europe PMC Funders Author Manuscripts

Europe PMC Funders Author Manuscripts

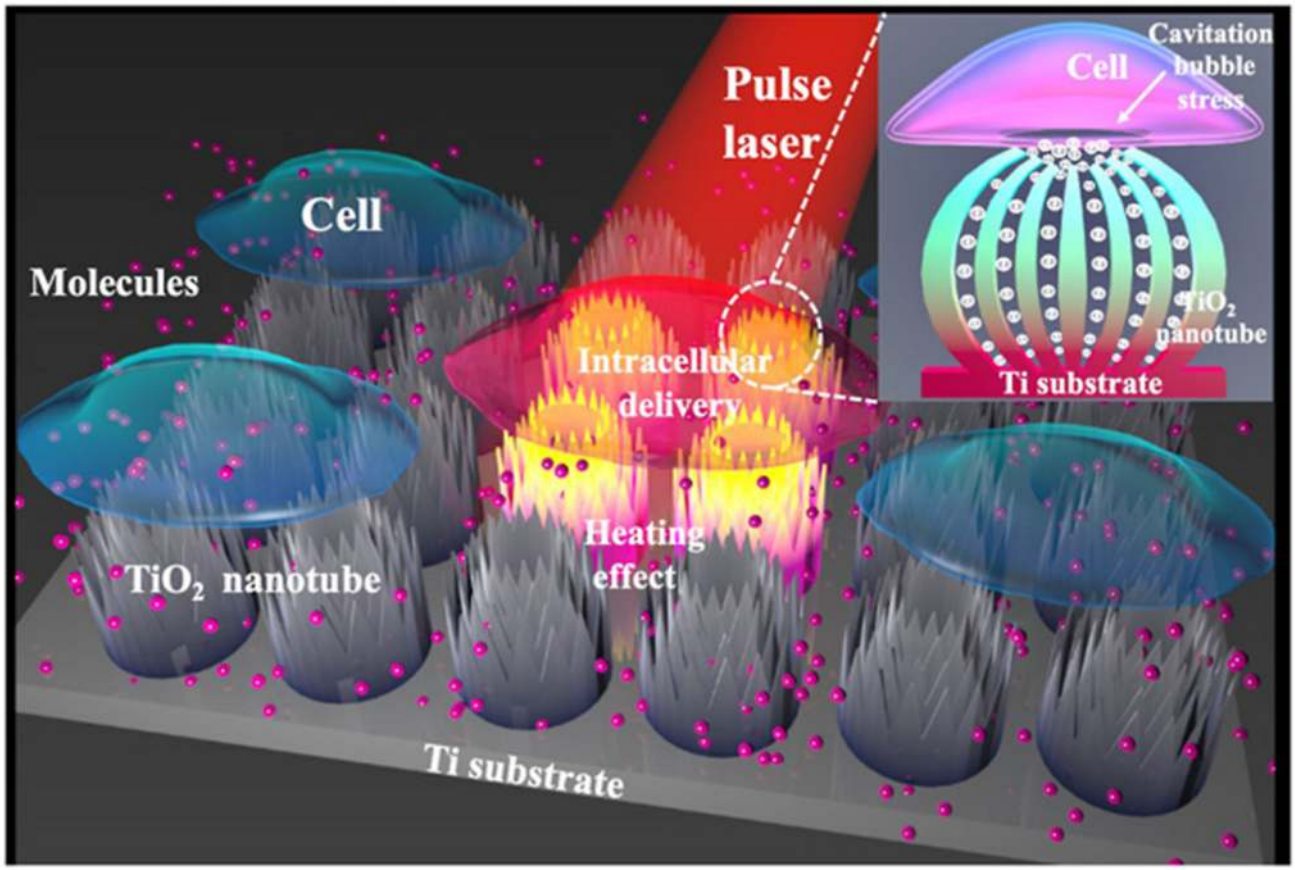

Graphical Abstract.

Keywords

Micro flowers; Nanotubes; Intracellular delivery; Photoporation; Nanosecond pulse laser; Delivery efficiency; Cell viability

The introduction of foreign biomolecules into cells through intracellular delivery, with high transfection efficiency and high cell viability, is a challenging task for therapeutics, diagnostics, and many biological and biomedical research [1,2]. Over the years, many transfection techniques have been developed, including biological, chemical, and physical methods [3–9]. The chemical and biological methods such as cationic polymers, cell-penetrating peptide, viral vectors have been widely used for intracellular delivery [6,7,10]; however, most of these techniques are limited with cell-specific plasmid delivery due to plasmid degradation, toxicity or safety concerns [11,12]. The physical methods such as microinjection [13], electroporation [8,14,15], jet injection [16], and sonoporation [17] have widely been developed, which use physical energy to disrupt the cell membranes and deliver foreign biomolecules into cells with high transfection efficiency and high cell viability. The microinjection technique can deliver biomolecules in all cell types with high transfection efficiency; however, it is a time-consuming process, limited with low throughput delivery,

and demands high skill person. The sonoporation technique uses shockwaves to deliver biomolecules into cells; however, it produces high toxicity and strong shear force that can cause cell damage easily and results in low cell viability [18]. In contrast, the electroporation technique is widely used for gene transfer due to its simplicity, short process time, and high throughput delivery; though, these techniques are often limited due to pH variation, easy sample contamination, toxicity, and electrolysis effect [8,19].

In the last two decades, the photoporation method has been emerging for a highly efficient intracellular delivery [20–26]. There are several techniques for photoporation mediated by light energy. Among them, a common methodology is the usage of metallic nanoparticles to interact with laser light and generate cavitation bubbles causing shear stress that deforms cell membrane and deliver biomolecules into cell. However, their delivery efficiency and viability need to be improved [27]. For photoporation, titanium (Ti) and Ti-based alloys can be a good choice due to their cost-effectiveness and easy to fabricate. Moreover, it exhibits superior mechanical properties, high corrosion resistance, and good biocompatibility [28,29]. Here, we proposed a proof-of-concept TiO_2 micro-flowers-based photoporation platform for intracellular delivery. Each TiO_2 micro-flower consists of a branch of TiO_2 nanotubes arranged in a flower-like manner on top of Ti substrate. Upon pulse laser irradiation, Ti substrate heat-up and induces vapor bubbles due to heating. The bubbles grow through TiO_2 nanotubes, and finally disrupt the cell membrane, which allows molecular delivery. Fig. 1 shows the schematic of this delivery process. The results show highly efficient intracellular Propidium iodide (PI) dye delivery (93%) into HCT cells with cell viability ~ 98%. This newly invented and highly biocompatible optoporation platform can be adapted as standard, safe, and cost-effective methods to perform intracellular delivery.

The TiO_2 micro-flowers were fabricated on titanium substrate using the electrochemical anodization technique. The detailed anodization and fabrication process are illustrated in supplementary materials. Fig. 2 (a) shows the field emission scanning electron microscopy (FESEM) image of the fabricated TiO_2 micro-flowers. A single micro-flower diameter is approximately 35–40 μm and inter-flower distance ~10–15 μm with height ~2.5–3 μm. The micro-flower construct with a branch of petals, and each petal thickness is approximately 300–400 nm. Again each petal is a construct of the branch of TiO_2 nanotubes, which is shown in Supplementary Figure. S1 Each TiO_2 nanotubes have approximately 60–80 nm diameter with 400 nm height. Fig. 2b shows a higher magnification image of Fig. 2a. Fig. 2 (c) and (d) show 3D construction images from FESEM image. The images confirm the high degree of ordering of the micro flowers. The detailed characterization techniques such as Fourier transform infrared spectroscopy (ATR-FTIR), Raman spectra and EDS confirm the TiO_2 microstructure formation on titanium substrate. ATR-FTIR, Raman spectra and EDS data with detailed explanations (Fig. S2 and S3 and Table 1) are provided in the supplementary material.

After micro-flowers fabrication, the device was cleaned with the standard cleaning process and treated under ultraviolet light for 2 h for sterilization. Afterward, the device was cleaned using ultrapure water (18 MΩ) to remove the contaminations from the device surface. After introducing the cells with medium, the device was transferred into an incubator (37 °C with 5% CO_2) overnight to obtain proper cell adhesion on top of the device surface. The detailed

cell culture protocol is provided in the supplementary material. Supplementary Figure (S4 shown calcein-AM staining (cell-permeable dye produce green color for live cells) live cells have adhered on top of the microflower surface as monolayer and it confirm that cells were grown healthy in nature. When cells strongly adhere to the micro-flower device surface, then cell impermeable molecules were added onto the device, and pulse laser was exposed for photoporation experiment.

In our study, first, PI dye was added on device surface (without adding any other dye), then 6.5 mJ laser energy with 5 ns pulse duration at 680 nm wavelength, with 10 Hz pulsing frequency was irradiated on the sample and finally the device was scanned at a speed of 150 mm/min. The PI dye is cell impermeable, and it can deliver into cell cytosol and produce red fluorescence imaging only if any mechanical membrane rupture happens [30]. Here due to pulsed laser irradiation, the Ti substrate heats-up and produces vapor bubbles. These bubbles can rapidly grow, coalesce and collapse to induce explosion resulting in very strong fluid flow through the branch of nanotubes in each petal of micro-flower and finally disrupt the cell plasma membrane to create transient membrane pores. As a result, PI dye was successfully delivered into the cells from outside by a simple diffusion process, due to concentration variation. Fig. 3a shows the successful PI dye delivery into HCT cells with 93% delivery efficiency. To check if the cells are alive or dead (because PI dye also can stain the nucleus of dead cells) after delivery, we added Calcein AM after 5 h of laser exposure. The calcein-AM hydrolysis inside live-cell and produce green fluorescence; in contrast, no color is generated for dead cells. Fig. 3b shows the live-cell imaging using calcein-AM (green). Fig. 3c shows the merged image of both (Fig. 3 a,b) distinguishing live and dead cells. Most of the cells of this image are green to yellowish-green color, indicating that cells are highly viable after delivery and very few red colors appear due to dead cells. Thus, these figures confirm that, after delivery, most of the cells are alive, and the cell viability reached approximately 98%.

In order to affirm bubble generation, we perform COMSOL multiphysics simulation that gives a clear picture of light-induced heating in this device. Since the micro-flower surface shows complete wettability (contact angle ~0°), each nanotube within the flower is considered to be filled by water medium in this simulation. We have simulated a model system (shown in supporting information Figure S5) containing four nanotube arrays on Ti substrate. Each nanotube has an outer diameter of 60 nm, thickness 10 nm and height 80 nm. This model has been simulated for laser excitation at 680 nm with a pulse duration of 5 ns and fluence 35 mJ/cm^2. After irradiating with nanosecond laser pulse, the Ti substrate absorbs the laser energy and acts as a transient heat generator [31]. The simulation result shows local electric field enhancement in-between the nanotubes' nano-spaces near the Ti metallic substrates, as shown in Fig. 4a. This observation is similar to the local field enhancement at the nano-gap between the metallic substrate and dielectric nanoparticle [32,33]. Resistive heatings, as shown in Fig. 4b, is more at Ti/TiO_2 interface compare to bare Ti substrate without nanotubes. Half part of water on the Ti substrate is visually inactivated to show the heat distribution across the nanotubes in Fig. 4b. This happens due to confinement of more electric field at the nanogap in-between the TiO_2 nanotubes. It shows that heating occurs at the top surface of the Ti substrate due to its metallic characteristics. No heating effect is observed for TiO_2 nanotubes because the excitation energy (680 nm) is far

below the bandgap energy (3.2 eV) of TiO_2. The heat flux diffuses to the adjacent TiO_2 micro/nanostructures and the confined water medium with time. Once the local Ti/water temperature rises above the critical temperature [34] the vapor bubble nucleates within the nanotube (maybe at the dead-end at Ti/water interface). Local expansion of the nanostructures due to temperature can also help to nucleate the vapor bubble in nanochannel [35]. To calculate electron (T_e) and lattice temperature (T_l) in Ti substrate two-temperature model is used. The temperature dynamics for the whole model in time and space is obtained by following the equations below:

$$C_e(T_e)\frac{\partial T_e}{\partial t} = \nabla(k_e \nabla T_e) - g(T_e - T_l) + Q(t), \tag{1}$$

$$C_l\frac{\partial T_l}{\partial t} = \nabla(k_l \nabla T_l) + g(T_e - T_l) - g_{lw}(T_l - T_w) - g_{ln}(T_l - T_n), \tag{2}$$

$$\rho_n C_n\frac{\partial T_n}{\partial t} = \nabla(k_n \nabla T_n) + g_{ln}(T_l - T_n) - g_{nw}(T_n - T_w), \tag{3}$$

$$\rho_w C_w\frac{\partial T_w}{\partial t} = \nabla(k_w \nabla T_w) + g_{lw}(T_l - T_w) + g_{nw}(T_n - T_w) \tag{4}$$

Here, T_n is the nanotube temperature and T_w is the water temperature. g ~2×10^7 $Wm^{-3}K^{-1}$ is the electron-phonon coupling factor of Ti [36]. Electron thermal conductivity, k_e = 15.3 W/m.K, and lattice thermal conductivity, k_l = 5.2 W/m.K [37] of Ti. $g_{ab}(T_a - T_b)$ is the heat transfer from a to b medium with g_{ab} being boundary heat exchange with Ti/water interface, $g_{lw} = 105 \times 10^6$ W/m^2K, Ti/TiO_2 interface $g_{ln} = 1725 \times 10^6$ W/m^2K and TiO_2/water interface $g_{nw} = 68 \times 10^6$ W/m^2K, calculated following Ref [38]. $C_e = \alpha T_e$ is electronic specific heat [36] with α = 328.9 J m^{-3} K^{-2} and $C_l = 2.3 \times 10^6$ J m^{-3} K^{-1} is lattice specific heat of Ti [39]. C_w = 4182 J kg^{-1} K^{-1} and C_n = 639 J kg^{-1} K^{-1} are the heat capacities of water and TiO_2 nanotube [40], respectively. The mass density is ρ_w = 1000 kg m^{-3} of water and ρ_n = 4260 kg m^{-3} of TiO_2, respectively. Q(t) is transient heating due to pulsed laser irradiation. Fig. 4c shows the spatial temperature distribution across the whole model at the peak of temperature transient as shown in Fig. 4d. It shows that temperature maximizes at the upper surface of Ti and decreases gradually in both upper and lower directions. Interestingly, the temperature rise in Ti–TiO_2-water region is faster than Ti-water region because TiO_2 nanotubes act as a heat transfer medium for the former case (since $g_{ln} > g_{lw}$). The transient temperature dynamics, in Fig. 4d, shows that the water temperature rises far above the boiling point of water. Therefore, such high rise of water temperature can generate vapor bubbles and induce cavitation. Also, TiO_2 tube wall would experience the local expansion due to temperature rise (it is not included in the simulation). Such expansion can promote nucleation of cavitation bubble within nanotubes [35].

The previous studies conducted on confined liquids in micro-nanochannel showed that bubble initially starts with spherical shape and then expands until it occupies the whole cross-section of the tube, after which it grows preferentially in the axial direction [41]. The shape of the bubble occupies the majority of the cross-section of the tube, finally reaches the

cooler end of the tube [41]. Since the bubbles are bound to expand through the quasi-one-dimensional geometry of the tubes, flower-like shapes, drives the nano-bubbles towards the same spot of the membrane. This region is preferentially the interface of the top center of micro-flower and cell membrane. The collective growth and collapse of the bubbles at the same spot can significantly enhance shear stress and jet flow of the liquid causing local deformation of cell membrane. Thus, the peculiar arrangements of nanotubes in the micro flower petals provide a competent means to focus mechanical energy on a micron-size small region of the cell to produce a highly localized shear stress and strain, causing localized membrane deformation or poration. A very recent study presents a rigorous assessment on the impact of laser-induced bubble hydrodynamics on membrane deformation [42]. A varying bio-effects, including necrosis, apoptosis, repairable poration and survival have been observed. These distinct impacts were strongly dependent on the inter-distance between the spot of bubble generation and the cell membrane and bubble shape. The dynamical characteristics of tandem bubble and spherical bubble showed significantly distinguished bio-effect on cell membrane. While spherical bubble leads to uniform membrane deformation causing multiple pores at different position of the membrane, tandem bubble causes heterogeneous pinpoint membrane poration. This was attributed to a jet caused by asymmetric collapse of the tandem bubble leading to the splashing radial outflow or the exponentially decaying shear stress generated by the rapid expansion of the bubble [42]. A quantitative and detailed study of this bubble dynamics is beyond the interest of the present work. It is important to note that we observed a significantly improved cell viability ~98% compared to the previous studies on laser-induced intracellular delivery. This observation can be attributed to the fact that the pores get resealed after intracellular delivery without inducing permanent deformation. The previous studies showed that the distance between the bubble generating position and cell membrane plays a crucial role to decide which bio-effect would be more significant than the others. The fixed height of the TiO_2 nanotubes provides a safe distance to the cell so that the shear stress due to rapid expansion of the bubble at the point of nucleation cannot cause significant necrosis or apoptosis. Besides, the extremely high biocompatible surface of TiO_2 micro flowers can assist the cells to live longer which is the additional benefit for promoting high cell viability.

Furthermore, we have performed cell viability test on different days using TiO_2 micro-flowers. The viability was conducted as a control experiment using normal cell culture Petri dish without TiO_2 micro-flower, before and after laser exposure with TiO_2 micro-flower. The MTT "(3- [4,5-dimethylthiozol-2-yl]-2,5 diphenyl tetrazolium bromide, analytical grade, TCI, Japan)" assay was used for cell viability test using HeLa cells and the method defined in earlier studies [43]. For this test, initially, each sample was added in a 30 mm cell culture plate, and HeLa cells were seeded at a density of 0.5×10^5 cells/mL. The MTT assay test was performed after 2 h, 3 days, and 7 days before and after laser exposure. The concentration of 50 μl of 5 mg/ml, MTT (stock) was added in each plate and then incubated at a temperature of 37 °C in a 5% CO_2 incubator for 4 h. After 4 h, the cell culture medium containing MTT was removed from the culture plate by aspiration. Thereafter, the formed formazan crystals were dissolved by adding 500 μl dimethyl sulfoxide (DMSO, Sigma-Aldrich). Then, the 200 μl of DMSO dissolved formazan crystals aliquots were transferred into a 96-well plate for reading the optical density at 570 nm through a plate reader (AS

ONE MPR-A 100). All the samples were assayed in triplicates. The measured optical density relates to the viability of cells, higher the optical density, better the cell viability. Fig. 5 shows the cell viability using MTT assay with a control experiment, before and after laser exposure for 2 h, 3 days, and 7 days. It was observed that, with laser exposure on TiO_2, the cell viability was more than 96% after 2 h and continuously increase this viability even after 7 days.

In summary, we demonstrate a new proof of concept of pulsed laser activated intracellular delivery using TiO_2 micro-flowers. The micro-flowers were fabricated using electrochemical anodization process, which consists of a branch of TiO_2 nanotubes on each micro-flowers petals. Due to pulse laser activation and bubble generation, strong fluid flow induces on plasma membrane and creates transient membrane pores for intracellular delivery. Using our platform, we successfully deliver molecular dyes with high delivery efficiency and high cell viability. Our platform might be potentially applicable to basic cellular research, therapy, diagnostics, and biomedical research purpose.

Supplementary Material

Refer to Web version on PubMed Central for supplementary material.

Acknowledgments

We greatly appreciate for the financial support from DBT/Wellcome Trust India Alliance Fellowship under grant number IA/E/16/ 1/ 503062. The authors would like to thank Dr. Pallavi Gupta and Ms. B. Nandhini, for their help during experiments.

References

[1]. Pack DW, Hoffman AS, Pun S, Stayton PS. Design and development of polymers for gene delivery. Nat Rev Drug Discov. 2005; 4:581–593. DOI: 10.1038/nrd1775 [PubMed: 16052241]

[2]. Gu Z, Biswas A, Zhao M, Tang Y. Tailoring nanocarriers for intracellular protein delivery. Chem Soc Rev. 2011; 40:3638–3655. DOI: 10.1039/c0cs00227e [PubMed: 21566806]

[3]. Hima, M, Pallavi, G, Mohan, L, Nagai, M, Wankhar, S, Santra, TS. Microneedles-current trends & applicationsMicrofluid Bio-MEMS Devices Appl. Santra, TS, editor. Jenny Stanford Publisher Pvt. Ltd; Singapore: 2020. 68

[4]. Shinde, P, Kumar, A, KavithaDey, K, Mohan, L, Kar, S, Barik, TK, Sharifi-Rad, J, Nagai, M, Santra, TS. Physical approaches for drug deliveryDeliv Drugs. Elsevier; 2020. 161–190.

[5]. Shinde P, Mohan L, Kumar A, Dey K, Maddi A, Patananan AN, Tseng FG, Chang HY, Nagai M, Santra TS. Current trends of microfluidic single-cell technologies. Int J Mol Sci. 2018; 19 doi: 10.3390/ijms19103143

[6]. Nayak S, Herzog RW. Progress and prospects: immune responses to viral vectors. Gene Ther. 2010; 17:295–304. DOI: 10.1038/gt.2009.148 [PubMed: 19907498]

[7]. Schmid RM, Weidenbach H, Draenert GF, Liptay S, Lührs H, Adler G. Liposome mediated gene transfer into the rat oesophagus. Gut. 1997; 41:549–556. DOI: 10.1136/gut.41.4.549 [PubMed: 9391258]

[8]. Kar S, Mohan L, Dey K, Shinde P, Chang HY, Nagai M, Santra TS. Single-cell electroporation: current trends, applications and future prospects. J Micromech Microeng. 2018; 28 123002 doi: 10.1088/1361-6439/AAE5AE

[9]. Kumar, A, Mohan, L, Shinde, P, Chang, HY, Nagai, M, Santra, TS. Mechanoporation: toward single cell approachesSingle-Cell Technol. Hand, B, editor. Springer Singapore; 2018. 1–29.

[10]. Stephens DJ, Pepperkok R. The many ways to cross the plasma membrane. Proc Natl Acad Sci U S A. 2001; 98:4295–4298. DOI: 10.1073/pnas.081065198 [PubMed: 11274366]

[11]. Crystal RG. Transfer of genes to humans: early lessons and obstacles to success. Science. 1995; 270:404–410. DOI: 10.1126/science.270.5235.404 [PubMed: 7569994]

[12]. Hartman ZC, Appledorn DM, Amalfitano A. Adenovirus vector induced innate immune responses: impact upon efficacy and toxicity in gene therapy and vaccine applications. Virus Res. 2008; 132:1–14. DOI: 10.1016/j.virusres.2007.10.005 [PubMed: 18036698]

[13]. Capecchi MR. High efficiency transformation by direct microinjection of DNA into cultured mammalian cells. Cell. 1980; 22:479–488. [PubMed: 6256082]

[14]. Santra, TS, Wang, PC, Tseng, FG. Electroporation based drug delivery and its applicationsAdv Micro/Nano Electromechanical Syst Fabr Technol. InTech; 2013.

[15]. Santra TS, Kar S, Chang HY, Tseng FG. Nano-localized single-cell nano-electroporation. Lab Chip. 2020; 20:4194–4204. DOI: 10.1039/d0lc00712a [PubMed: 33047768]

[16]. Fuller DH, Loudon P, Schmaljohn C. Preclinical and clinical progress of particle-mediated DNA vaccines for infectious diseases. Methods. 2006; 40:86–97. DOI: 10.1016/j.ymeth.2006.05.022 [PubMed: 16997717]

[17]. Ohta S, Suzuki K, Ogino Y, Miyagawa S, Murashima A, Matsumaru D, Yamada G. Gene transduction by sonoporation. Dev Growth Differ. 2008; 50:517–520. DOI: 10.1111/j.1440-169X.2008.01026.x [PubMed: 18430029]

[18]. Lentacker I, De Cock I, Deckers R, De Smedt SC, Moonen CTW. Understanding ultrasound induced sonoporation: definitions and underlying mechanisms. Adv Drug Deliv Rev. 2014; 72:49–64. DOI: 10.1016/j.addr.2013.11.008 [PubMed: 24270006]

[19]. Santra TS, Tseng FG. Recent trends on micro/nanofluidic single cell electroporation. Micromachines. 2013; 4:333–356.

[20]. Wu YC, Wu TH, Clemens DL, Lee BY, Wen X, Horwitz MA, Teitell MA, Chiou PY. Massively parallel delivery of large cargo into mammalian cells with light pulses. Nat Methods. 2015; 12:439. [PubMed: 25849636]

[21]. Santra TS, Kar S, Chen TC, Chen CW, Borana J, Lee MC, Tseng FG. Nearinfrared nanosecond-pulsed laser-activated highly efficient intracellular delivery mediated by nano-corrugated mushroom-shaped gold-coated polystyrene nanoparticles. Nanoscale. 2020; 12:12057–12067. DOI: 10.1039/D0NR01792B [PubMed: 32469040]

[22]. Shinde P, Kar S, Mohan L, Chang HY, Tseng FG, Nagai M, Santra TS. Infrared pulse laser activated highly efficient intracellular delivery using titanium micro-dish device. ACS Biomater Sci Eng. 2020; doi: 10.1021/acsbiomaterials.0c00785

[23]. Ishii A, Hiruta Y, Heinemann D, Heisterkamp A, Kanazawa H, Terakawa M. Intracellular localization and delivery of plasmid DNA by biodegradable microsphere-mediated femtosecond laser optoporation. J Biophot. 2017; 10:1723–1731. DOI: 10.1002/jbio.201600323

[24]. Terakawa M, Tanaka Y. Dielectric microsphere mediated transfection using a femtosecond laser. Opt Lett. 2011; 36 2877 doi: 10.1364/ol.36.002877 [PubMed: 21808344]

[25]. Mohan L, Kar S, Hattori Ren, Ishii-Teshima M, Bera P, Roy S, Santra TS, Shibata T, Nagai M. Can titanium oxide nanotubes facilitate intracellular delivery by laser-assisted photoporation? Appl Surf Sci. 2021; 543 148815 doi: 10.1016/j.apsusc.2020.148815

[26]. Mohan L, Kar S, Mahapatra PS, Nagai M, Santra TS. Fabrication of TiO2microspikes for highly efficient intracellular delivery by pulse laser-assisted photoporation. RSC Adv. 2021; 11:9336–9348. DOI: 10.1039/d0ra09785c

[27]. Santra, Tuhin Subhra; Tseng, Fan-Gang. Handbook of Single Cell Technologies. first ed. Springer; Singapore: 2021.

[28]. Kaur M, Singh K. Review on titanium and titanium based alloys as biomaterials for orthopaedic applications. Mater Sci Eng C. 2019; 102:844–862. DOI: 10.1016/j.msec.2019.04.064

[29]. Mohan L, Anandan C. Wear and corrosion behavior of oxygen implanted biomedical titanium alloy Ti-13Nb-13Zr. Appl Surf Sci. 2013; 282:281–290. DOI: 10.1016/j.apsusc.2013.05.120

[30]. Santra TS, Chen CW, Chang HY, Tseng FG. Dielectric passivation layer as a substratum on localized single-cell electroporation. RSC Adv. 2016; 6:10979–10986.

[31]. Wu TH, Teslaa T, Teitell MA, Chiou PY. Photothermal nanoblade for patterned cell membrane cutting. Opt Express. 2010; 18:23153–23160. [PubMed: 21164656]

[32]. Hutter T, Huang FM, Elliott SR, Mahajan S. Near-field plasmonics of an individual dielectric nanoparticle above a metallic substrate. J Phys Chem C. 2013; 117:7784–7790. DOI: 10.1021/jp400963f

[33]. Li L, Hutter T, Finnemore AS, Huang FM, Baumberg JJ, Elliott SR, Steiner U, Mahajan S. Metal oxide nanoparticle mediated enhanced Raman scattering and its use in direct monitoring of interfacial chemical reactions. Nano Lett. 2012; 12:4242–4246. DOI: 10.1021/nl302029p [PubMed: 22765890]

[34]. Bao B, Zandavi SH, Li H, Zhong J, Jatukaran A, Mostowfi F, Sinton D. Bubble nucleation and growth in nanochannels. Phys Chem Chem Phys. 2017; 19:8223–8229. DOI: 10.1039/c7cp00550d [PubMed: 28271101]

[35]. Duan C, Karnik R, Lu MC, Majumdar A. Evaporation-induced cavitation in nanofluidic channels. Proc Natl Acad Sci U S A. 2012; 109:3688–3693. DOI: 10.1073/pnas.1014075109 [PubMed: 22343530]

[36]. Lin Z, Zhigilei LV, Celli V. Electron-phonon coupling and electron heat capacity of metals under conditions of strong electron-phonon nonequilibrium. Phys Rev B. 2008; 77 075133 doi: 10.1103/PhysRevB.77.075133

[37]. Powell RW, Tye RP. The thermal and electrical conductivity of titanium and its alloys. J Less-Commn Met. 1961; 3:226–233.

[38]. Chang G, Sun F, Duan J, Che Z, Wang X, Wang J, Kim MJ, Zhang H. Effect of Ti interlayer on interfacial thermal conductance between Cu and diamond. Acta Mater. 2018; 160:235–246. DOI: 10.1016/j.actamat.2018.09.004

[39]. Rao RR, Rajput A. Lattice specific heat and thermal expansion of titanium. Phys Rev B. 1979; 19:3323–3328. DOI: 10.1103/PhysRevB.19.3323

[40]. McDonald HJ, Seltz H. The heat capacities of titanium dioxide from 68-298°K. The thermodynamic properties of titanium dioxide. J Am Chem Soc. 1939; 61:2405–2407. DOI: 10.1021/ja01878a040

[41]. Sun C, Can E, Dijkink R, Lohse D, Prosperetti A. Growth and collapse of a vapour bubble in a microtube: the role of thermal effects. J Fluid Mech. 2009; 632:5–16. DOI: 10.1017/S0022112009007381

[42]. Yuan F, Yang C, Zhong P. Cell membrane deformation and bioeffects produced by tandem bubble-induced jetting flow. Proc Natl Acad Sci U S A. 2015; 112:E7039–E7047. DOI: 10.1073/pnas.1518679112 [PubMed: 26663913]

[43]. Mohan L, Kar S, Nandhini B, Dhilip Kumar SS, Nagai M, Santra TS. formation of nanostructures on magnesium alloy by anodization for potential biomedical applications. Mater Today Commun. 2020; 101403 doi: 10.1016/j.mtcomm.2020.101403

Europe PMC Funders Author Manuscripts

Europe PMC Funders Author Manuscripts

Highlights

- Titanium oxide micro-flowers (TMS) was formed on titanium by electrochemical anodization.
- TMS consists of branches of titanium dioxide nanotubes that play an essential role in efficient cargo delivery.
- Pulsed laser and TMS interaction generate cavitational bubbles and deform the cell membrane for intracellular delivery.
- Propidium Iodide dye was delivered into HCT cells with high delivery efficiency and cell viability.

Europe PMC Funders Author Manuscripts

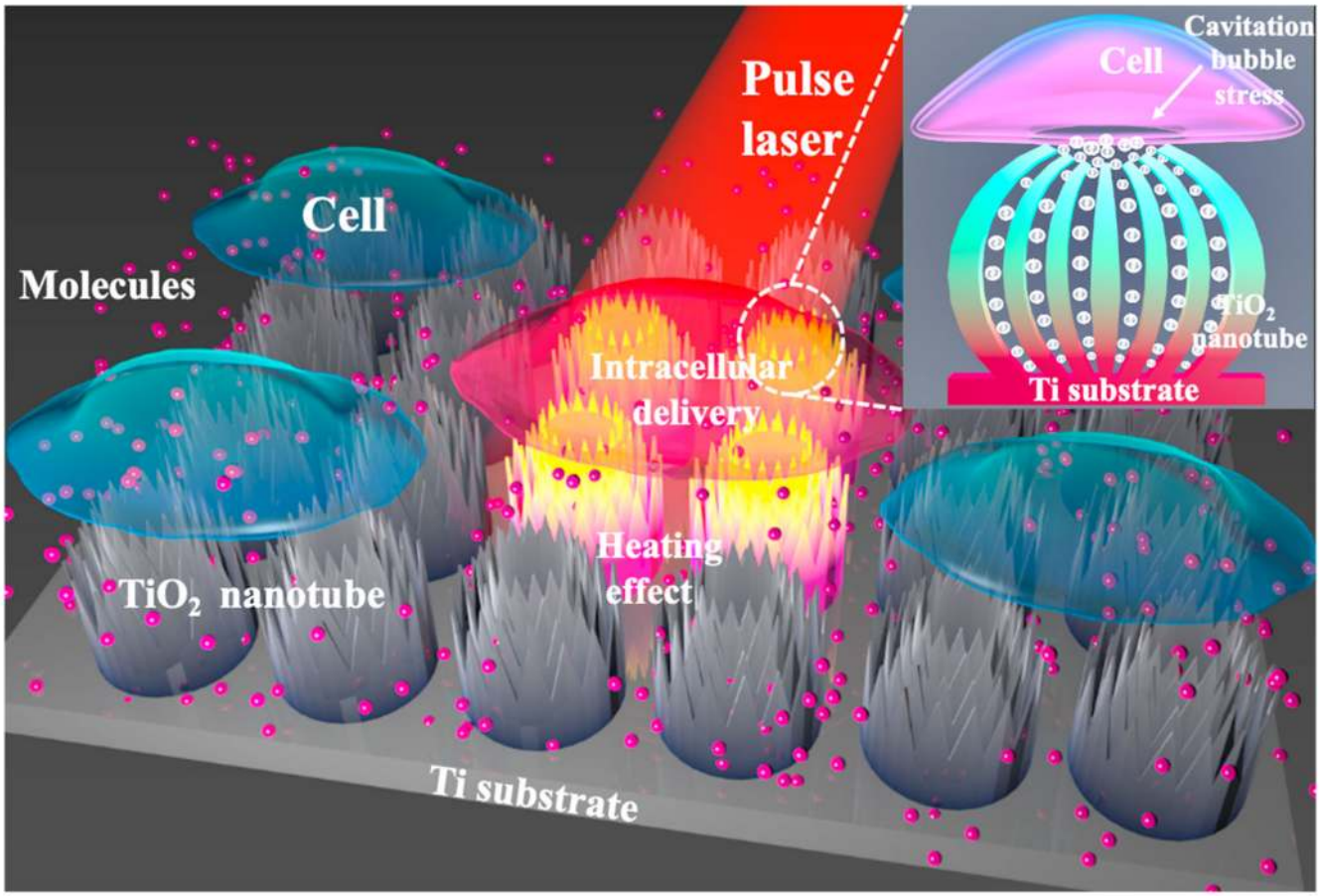

Fig. 1. The schematic of pulse laser-assisted vapor bubble generation and intracellular delivery using TiO_2 micro-flowers.

Europe PMC Funders Author Manuscripts

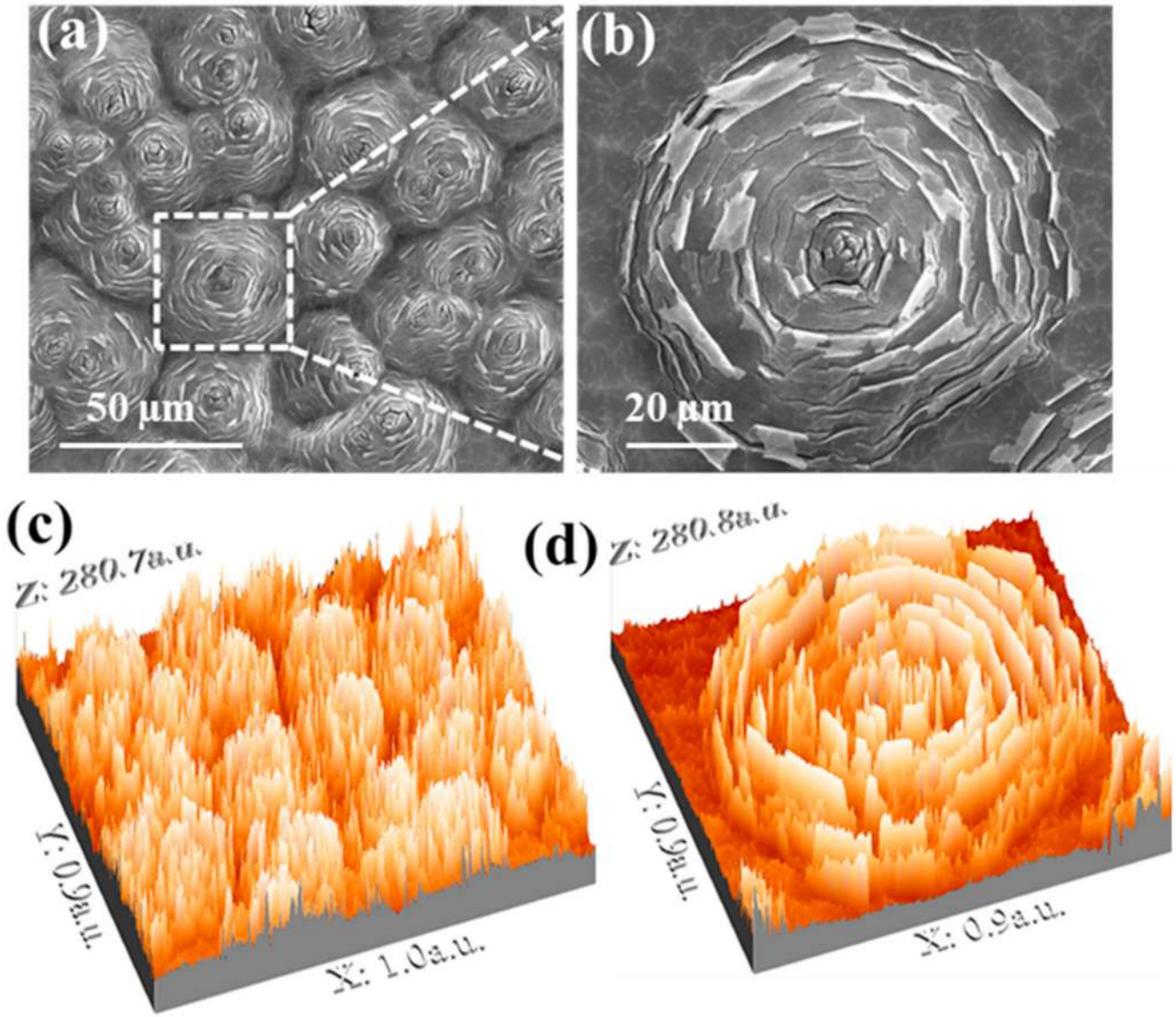

Fig. 2. The TiO_2 micro-flowers fabrication on Ti substrate using the electrochemical anodization technique.

(a) FESEM image of micro-flowers, (b) single microflower with higher magnification, (c) 3D construction of micro-flowers from the above FESEM image (d) single 3D construction of micro-flower.

Europe PMC Funders Author Manuscripts

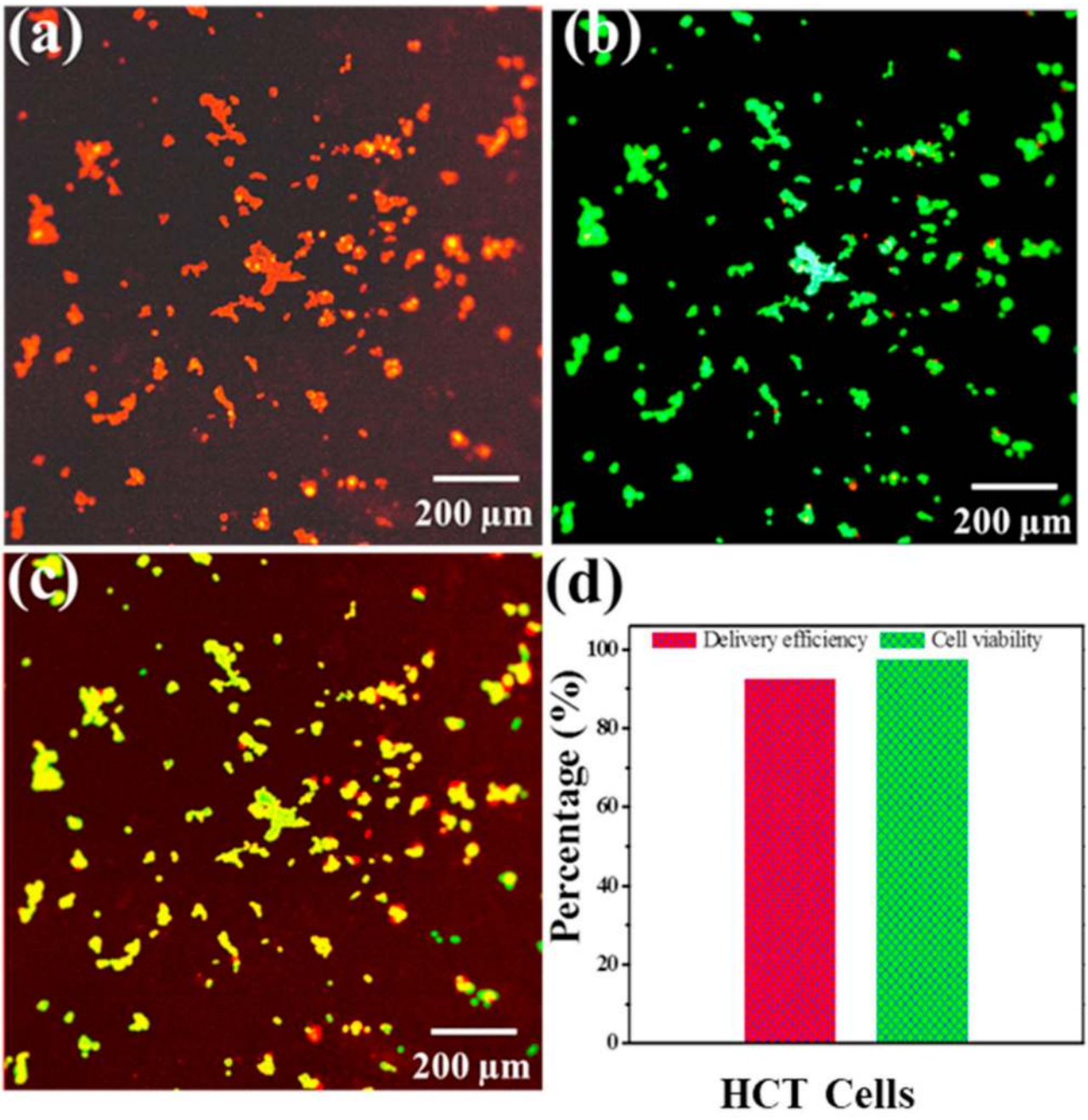

Fig. 3. PI dye delivery and cell viability of HCT cells at 680 nm wavelength with 6.5 mJ laser fluence

(a) PI dye delivery (red) (b) live-cell staining by Calcein AM (green) (c) merge image of live cells and PI dye delivery cells. (For interpretation of the references to color in this figure legend, the reader is referred to the Web version of this article.)

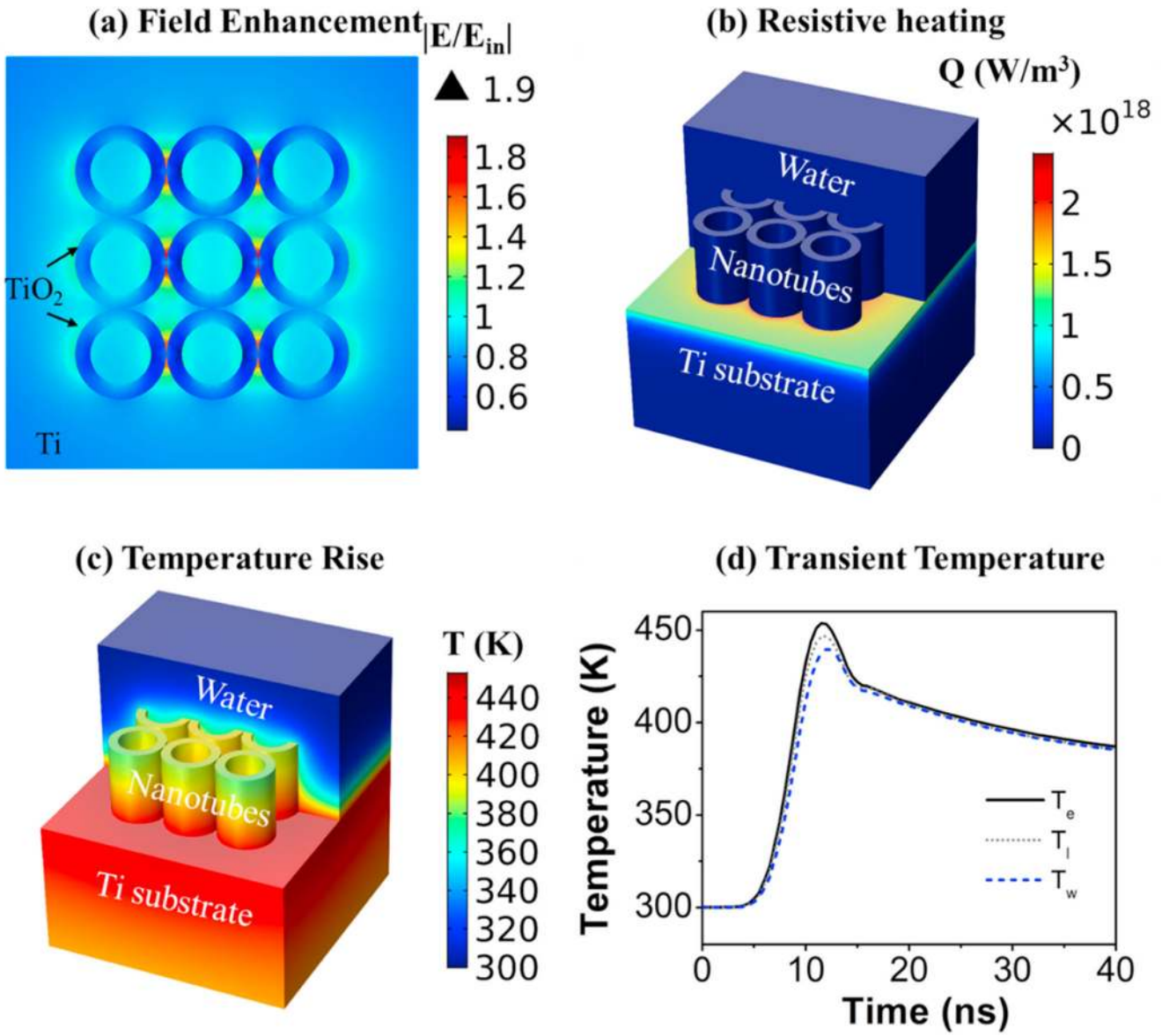

Fig. 4. Simulation results for TiO_2/Ti model.

(a) Field enhancement at nanospace in-between nanotubes close to the Ti substrate. (b) Resistive heating in 3D. (c) Spatial temperature distribution at the peak of transient temperature. (d) Transient dynamics of T_e, T_l, and T_w at an arbitrary position of Ti/water/TiO_2 interface.

Europe PMC Funders Author Manuscripts

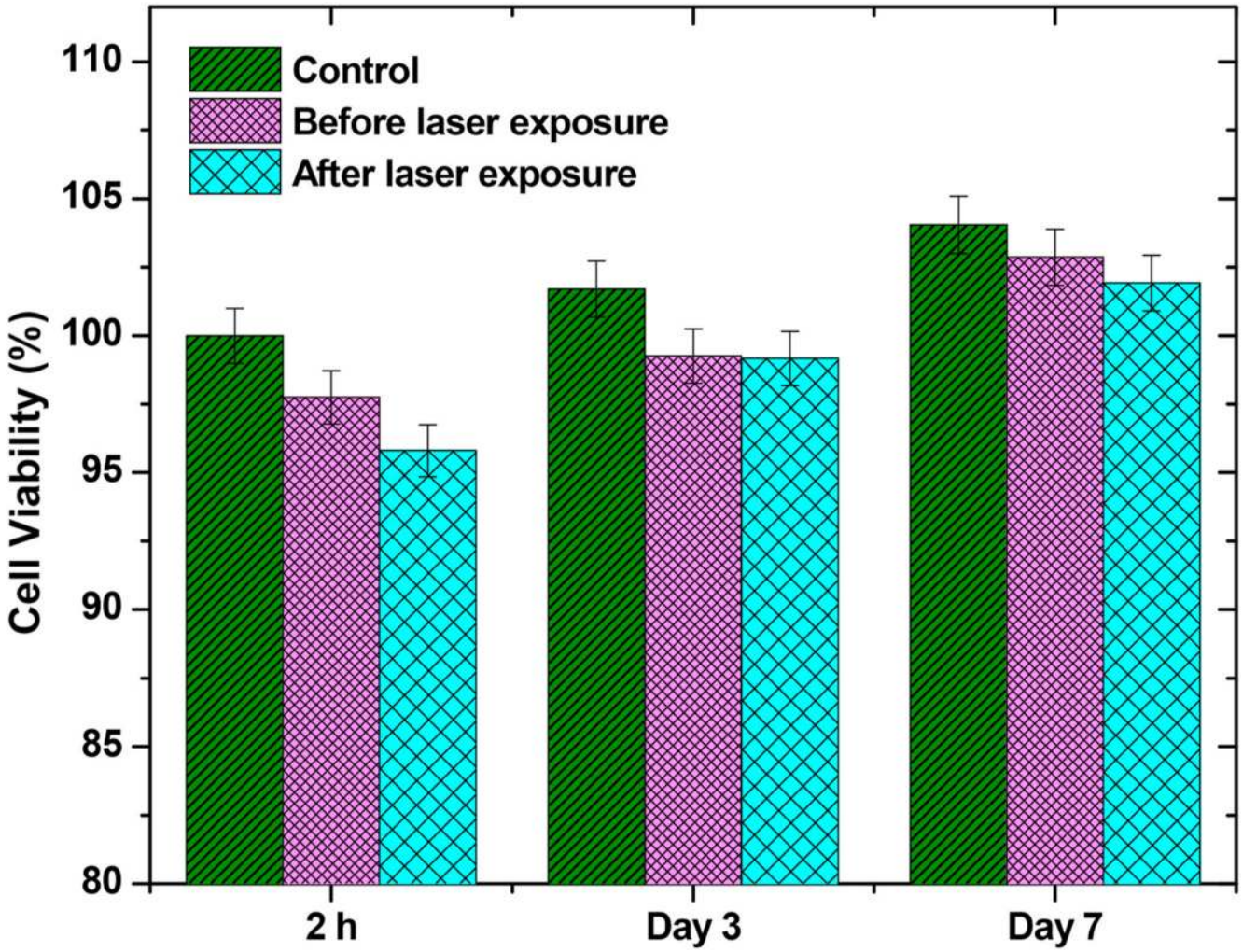

Fig. 5. Cell viability of HeLa cells using MTT assay on different days before and after laser exposure.